Chapter 2

Synthesis and Characterization of Nanoscale Molybdenum Sulfide Catalysts by Controlled Gas Phase Decomposition of $Mo(CO)_6$ and H_2S

Michael R. Close,[a] Jeffrey L. Petersen,[a] and Edwin L. Kugler[b]

[a]Department of Chemistry and
[b]Department of Chemical Engineering
West Virginia University, Morgantown, WV 26506-6045

Abstract

Molybdenum sulfide catalysts with surface areas ranging from 16 to 120 m^2/g were prepared by the thermal decomposition of $Mo(CO)_6$ and H_2S vapors in a specially designed tubular reactor system. The gas phase decomposition (GPD) reactions performed at 500 to 1100 C produced only MoS_2 when excess H_2S was used. The optimum temperature range for the high yield production of MoS_2 was from 500 to 700 C. By controlling the decomposition temperature, the $Mo(CO)_6$ partial pressure, or the inert gas flow rate, the surface area, oxidation state, chemical composition, and the grain size of the molybdenum sulfide product(s) were modified. At reactor temperatures between 300 and 400 C, lower valent molybdenum sulfide materials, which were sulfur deficient relative to MoS_2, were obtained with formal molybdenum oxidation states intermediate to those found for Chevrel phase compounds, $M'Mo_6S_8$ (M'=Fe, Ni, Co) and MoS_2. By lowering the H_2S flow rate used for the GPD reaction at 1000 C, mixtures containing variable amounts of MoS_2 and Mo_2S_3 were produced. Thus, through the modification of critical reactor parameters used for these GPD reactions, fundamental material properties were controlled.

Introduction

Conventional solid state syntheses are typically performed by mechanical mixing of the precursors, pressing the resultant reaction mixture into pellets, and then heating the pellets under inert or reactive gas conditions. This synthetic approach generally produces materials with low surface areas (often less than 1 m^2/g) and may afford a mixture of phases due to incomplete solid state diffusion. The utility of producing materials with higher surface areas and purity, while using lower reaction temperatures, has motivated researchers to investigate alternative molecular mixing methods including chemical vapor deposition,[1] sol-gel processing,[2] spray pyrolysis,[3] and co-precipitation.[4] These strategies rely on combining the requisite precursors on an atomic or molecular level *prior* to heat

processing, thus lowering solid state diffusional barriers and the energy requirements necessary for product formation. In addition, processing variables inherent to these techniques may provide synthetic control over fundamental material properties, such as the surface area, the chemical composition, and the crystallographic phase.

Precise control of product surface area, chemical composition, and crystallographic phase has significant application in the area of heterogeneous catalysis. Solid phase catalysts can be prepared in a variety of ways. For example, MoS_2 is an effective heterogeneous hydrogenation[5] and hydrodesulfurization[6] catalyst and has been used as a Fischer-Tropsch synthesis catalyst for the production of hydrocarbons, or alcohols when it is modified with alkali.[7] MoS_2 has been prepared by the thermolysis of MoS_3[7f, 8] and $(NH_4)_2MoS_4$,[7e, 9] by the solid-state metathesis reaction of $MoCl_5$ and Na_2S,[10] and by various molecular mixing approaches, such as laser pyrolysis,[11] liquid phase decomposition,[12] and CVD[13] using $Mo(CO)_6$ and different sulfiding agents. Recently, Tenne and co-workers[14] have employed the gas phase reaction of MoO_{3-x} and H_2S in a reducing H_2 atmosphere to produce a pure inorganic fullerene phase of MoS_2. Samples of MoS_2 prepared by these routes exhibit widely variable surface areas.

In conjunction with our efforts to develop efficient heterogeneous catalysts for the productions of higher alcohols, we decided to investigate the controlled gas phase decomposition (GPD) of $Mo(CO)_6$ and H_2S as a viable route for the generation of high surface area MoS_2. $Mo(CO)_6$ is well-suited for this purpose because the Mo(0) oxidation state eliminates the need to conduct the reaction in a reducing environment. Its inherent volatility further provides the flexibility of being able to alter the $Mo(CO)_6$ partial pressure in the reactive gas stream by simply varying the temperature used to sublime it.

In this paper, we describe the use of a continuous flow pyrolysis reactor for the production of MoS_2 by controlled gas phase decomposition of $Mo(CO)_6$ and H_2S. By varying the furnace temperature, the type of gas injection system, the carrier gas flow, and the $Mo(CO)_6/H_2S$ composition in the reaction stream, we have been able to optimize yields and more importantly influence the surface area, crystallographic phase, and chemical composition of the GPD products. Although care must be taken in correlating catalyst surface area with catalytic activity, oxygen titration studies coupled with BET measurements of the MoS_2 produced by our reactor show that the mass density of active sites is proportional to surface areas of these materials.[15] Specific details regarding the reactor design and the characterization of the molybdenum sulfide products by XRD, XPS, and SEM methods are also presented.

Experimental

Chemicals. $Mo(CO)_6$ was obtained from Strem Chemical Co. and purified by sublimation prior to use. H_2S (Matheson Gas Products) was used as received. He and Ar were purified by passage over supported copper and molecular sieves to remove oxygen and water, respectively.

Gas Phase Reactor. The reactor system illustrated in Figure 1 can be divided into three separate sections: sample introduction, sample pyrolysis, and material isolation. The sample

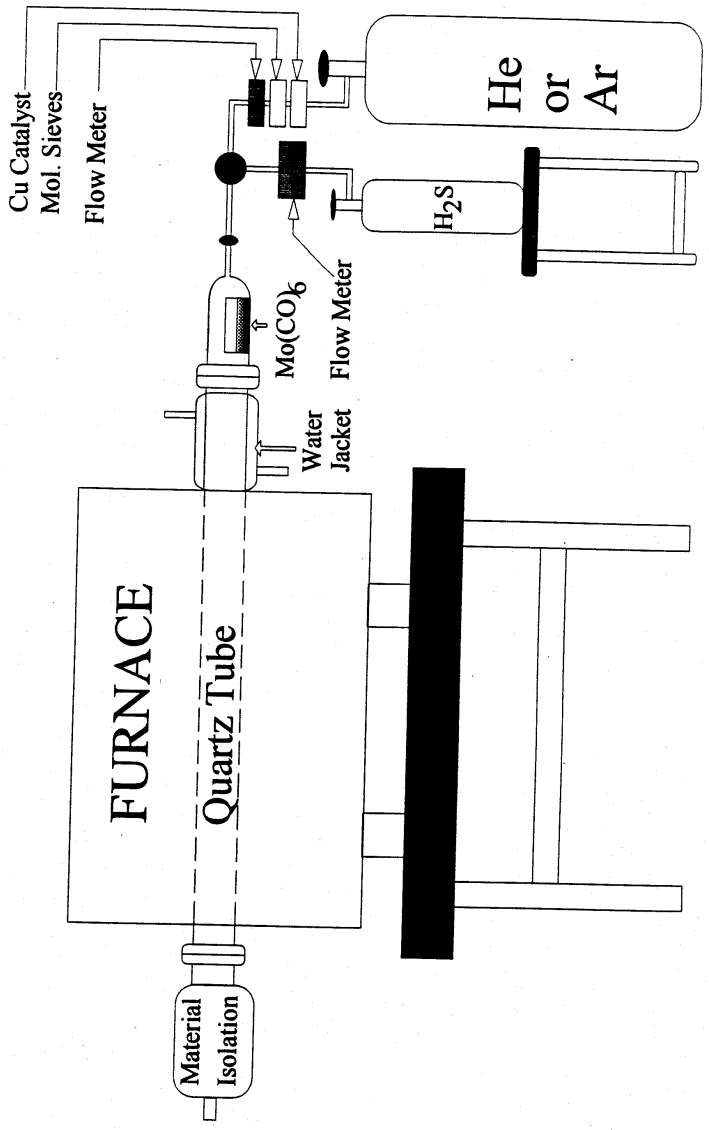

Figure 1. Gas phase reactor system used to form molybdenum sulfides. $Mo(CO)_6$ and H_2S vapor is mixed and then pyrolyzed in the furnace at temperatures from 300 to 1100 C to produce finely divided molybdenum sulfides. The nanoscale particles resulting from these decompositions are isolated in tubes constructed from course porosity filter paper.

pyrolysis and material isolation segments were the same for each experiment described in this investigation, while two different configurations were used for the sample introduction (see Figure 2). $Mo(CO)_6$ vapor was produced by heating the section of the reactor containing 2-3 grams of

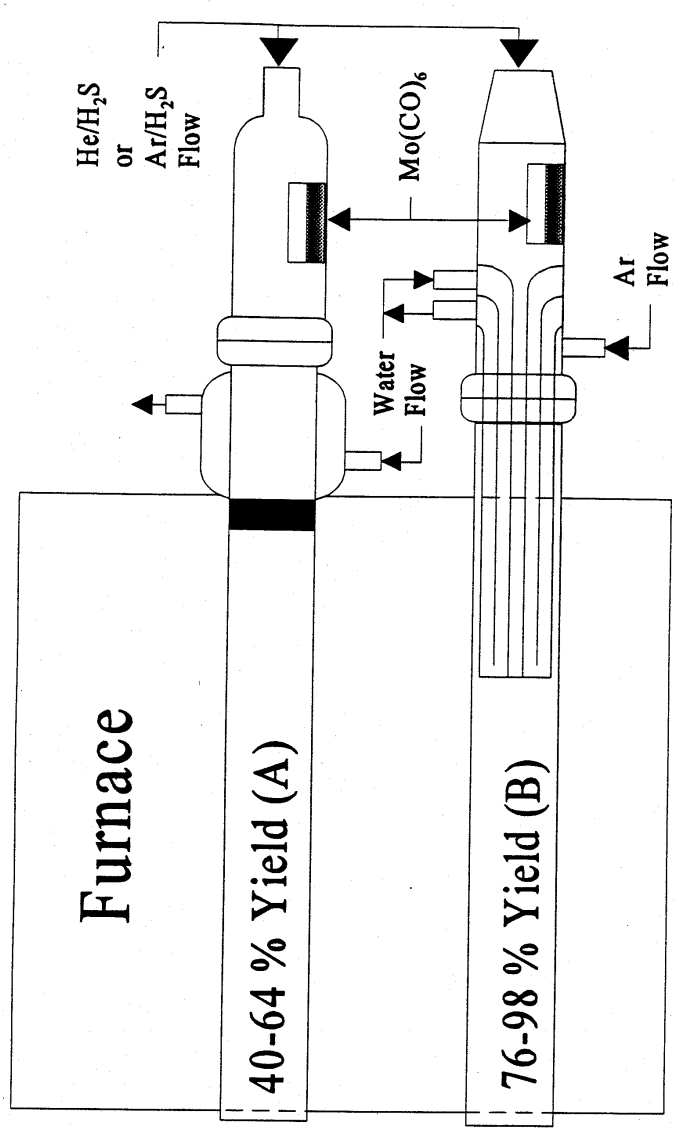

Figure 2. Two injector configurations used in the gas phase reactor. Reactor configuration A was used in initial experiments and produced relatively low yields due to metal decomposition on the quartz tube inner surface at the water jacket/furnace interface. Reactor configuration B was developed subsequently to increase the yield by reduction of material loss on the inner tube surface and to allow variation in the heating zone length by changing the relative position of the water-cooled injector within the furnace.

$Mo(CO)_6$ with either a heating tape (reactor configuration A) or a band heater (reactor configuration B). He, Ar and H_2S gas flow rates were measured by Matheson rotameters, which were locally calibrated. The reaction tube consisted of 25 mm fused silica tubing (3 foot length) with No. 25 O-ring quartz joints (G.M. Associates). The products were collected in filter tubes constructed from Fisher P8 course porosity filter paper. An optically clear glass disk was incorporated into the collection device to allow visual monitoring of the GPD reactions. $Mo(CO)_6$ vapor was introduced into the reactor

using either an outer (reactor configuration A) or an inner (reactor configuration B) water jacket injection system, both made of Pyrex. Configuration A was used initially whereas configuration B was developed later to increase material yields and to reduce annealing time. Configuration B consists of three concentrically aligned Pyrex tubes which provide water cooling of the gas flow tube up to 8 inches inside the furnace. An additional gas port was added in the design of configuration B to minimize the material loss on the fused silica tube surface by establishing a laminar flow of inert gas around the water-cooled injector. Both of the water jackets were maintained at the same temperature with a temperature-controlled circulating water bath. A 24" Lindberg split furnace controlled by a Eurotherm 818 programmable controller was used to heat the reaction tube.

$Mo(CO)_6$ Gas Phase Reactions. Three series of reactions were performed using reactor configuration A and reactor configuration B. Reactor configuration A was used in the first set of reactions to prepare four molybdenum sulfide samples by decomposing $Mo(CO)_6$ and H_2S vapors at 500 (A1), 800 (A2), 900 (A3), and 1100 C (A4). In a second series of GPD reactions of $Mo(CO)_6/H_2S$, eleven molybdenum sulfide samples were prepared using reactor configuration B at temperatures ranging from 300 to 900 C. A third study using configuration A was performed for the purpose of preparing lower valent molybdenum sulfides, samples C1 and C2, by lowering the H_2S flow rate. Experimental parameters for the GPD reactions are summarized in Table 1.

Table 1. Experimental Conditions and Yields for the Gas Phase Decompositions of $Mo(CO)_6$ and H_2S.

Run	$Mo(CO)_6$ mass (g)	T_f[a]	T_{Mo}[a]	T_{wj}[a]	Ar_i[a]	Ar_o[a]	H_2S rate (mL/min)	Yield %
A1	2.0	500	69	-	635	-	26	49.1
A2	2.0	800	69	-	549	-	26	64.3
A3	2.0	900	69	-	529	-	26	40.1
A4	2.0	1100	69	-	654	-	26	41.3
B1	3.0	300	98-99	85	220	700	11	26.7
B2	3.0	400	98-99	85	220	700	11	45.0
B3	3.0	500	98-99	85	220	700	11	82.7
B4	3.0	600	98-99	85	220	700	11	88.6
B5	3.0	700	98-99	85	220	700	11	95.0
B6	3.0	800	98-99	85	220	700	11	94.6
B7	3.0	900	98-99	85	220	700	11	98.2
B8	3.0	500	93	80	220	635	11	82.8
B9	3.0	500	104	80	220	635	11	82.8
B10	3.0	500	93	70	0.00	415	15	<20
B11	3.0	500	98-99	85	250	700	11	75.5
C1	2.0	1000	80	N/A	300	N/A	5	0.844 g[b]
C2	2.0	1000	80	N/A	300	N/A	2.5	0.779 g[b]

[a] T_f = furnace temperature; T_{Mo} = $Mo(CO)_6$ temperature; T_{wj} = temperature of the water jacket injection tube; Ar_i = argon flow rate (mL/min) through the inner tube containing the $Mo(CO)_6$; Ar_o = argon flow rate (mL/min) through the reaction tube outer section.
[b] Mixture of phases produced, therefore the amount given is the total product weight.

In a typical GPD reaction, $Mo(CO)_6$ powder (2.0 or 3.0 grams) was weighed into a cylindrical Pyrex boat and placed into the sample introduction section. The reactor system was assembled and purged with He (or Ar) and H_2S for 20-30 minutes. The H_2S flow was terminated and the furnace was heated to an operating temperature ranging from 300 to 1100 C at a rate of 1000 C/hr. When the temperature reached 100 C below the set point, the H_2S and inert gas flows were adjusted to the appropriate processing values. The water in the water jacket and the reservoir containing $Mo(CO)_6$ were heated to predetermined settings and the GPD reaction was allowed to proceed until all of the $Mo(CO)_6$ was depleted. The reaction time was approximately 1 hour per gram of $Mo(CO)_6$ consumed. Although the bulk molybdenum sulfide products do not appear to react in air, XPS data show that samples exposed to air contain more surface oxygen than

those stored under inert gas. The samples produced by reactor configuration A were stored under an inert nitrogen atmosphere, whereas the samples produced by reactor configuration B were exposed briefly to air prior to storage. The yields for these GPD reactions ranged from <20 to 98 %, depending on the reaction conditions. Temperature cycling studies, which involve the heating of the MoS_2 samples between 200 C and 400 C for 80 hours, show that their catalytic properties (activity/selectivity) remain unchanged and thereby indicate that these materials are stable to thermal treatment for an extended period of time over this temperature range.

Material Characterization. X-ray powder diffraction measurements were performed on a Philips PW 1800 diffractometer using Cu K radiation. The powders were loaded on zero background single crystal quartz disks[16] by either packing the samples into a cavity in the disk or by dispersing the powders in pentane and depositing the dispersion on the surface of the disk. Mo and S binding energies and ratios were determined by X-ray photoelectron spectroscopy performed on a Physical Electronic Industries 5600 XP using monochromatic Mg radiation. The binding energies were referenced to C(1s) = 284.8 eV. The sulfur compositions were determined by combustion analysis using a Leco SC-432DR instrument. A Perkin Elmer 2400 CHN combustion analyzer was used to determine the carbon percentages. BET surface areas were determined with nitrogen using a Coulter Omnisorb 360 instrument operated in a static adsorption mode. Equilibrium nitrogen adsorption was measured over the pressure range of 0 to 120 Torr (1 Torr = 1.33 x 10^2 Pa). The scanning electron micrographs were obtained on a JOEL 6300L Field Emission SEM located in the WVU Department of Geology. Results $Mo(CO)_6/H_2S$ Decompositions with Reactor Configuration A. In the initial series of GPD reactions, molybdenum sulfide samples were prepared by reacting $Mo(CO)_6$ and H_2S vapors at 500 (A1), 800 (A2), 900 (A3), and 1100 °C (A4) using reactor configuration A. The results summarized in Tables 1 and 2 indicate that the MoS_2 surface area decreased significantly from

Table 2. Analytical Data for the MoS_2 Samples Prepared by the GPD of $Mo(CO)_6$ and H_2S with Reactor Configuration A.

Run	T_f (°C)[a]	Binding Energies (eV)				S/Mo (XPS)	Yield %	XRD[b] FWHH	Surface Area (m^2/g)	Sulfur % (Carbon %)
		Mo $3d_{3/2}$	Mo$3d_{5/2}$	S $2p_{1/2}$	S $2p_{3/2}$					
A1	500	232.4	229.2	163.2	162.1	2.34	49.9	2.4	82.0	38.85 (0.05)
A2	800	232.4	229.3	163.4	162.2	2.11	64.3	2.0	57.4	56.9 (<0.01)
A3	900						40.6	1.6	29.6	48.7 (<0.01)
A4	1100	232.4	229.2	163.3	162.1	1.94	41.3	1.3	16.7	49.4 (<0.01)

[a] Furnace temperature.

[b] Full width at half height measurement in 2 for the Bragg powder diffraction peak for the (0 0 2) reflection.

82.0 to 16.7 m^2/g as the furnace temperature was increased from 500 to 1100 C, respectively. The scanning electron micrographs of samples A1 and A4 shown in Figure 3 indicate that the

Figure 3(a)

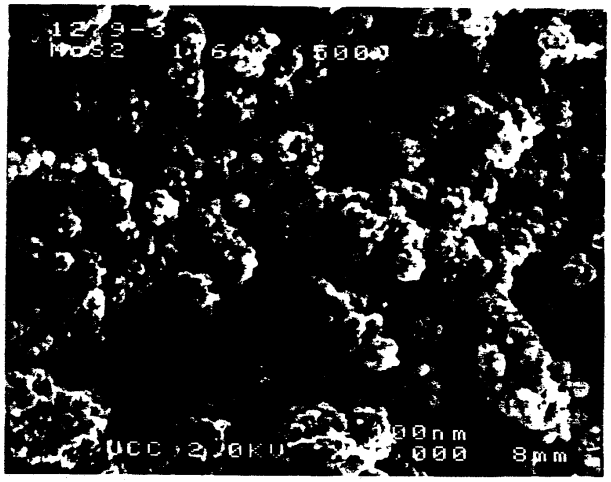

Figure 3(b)

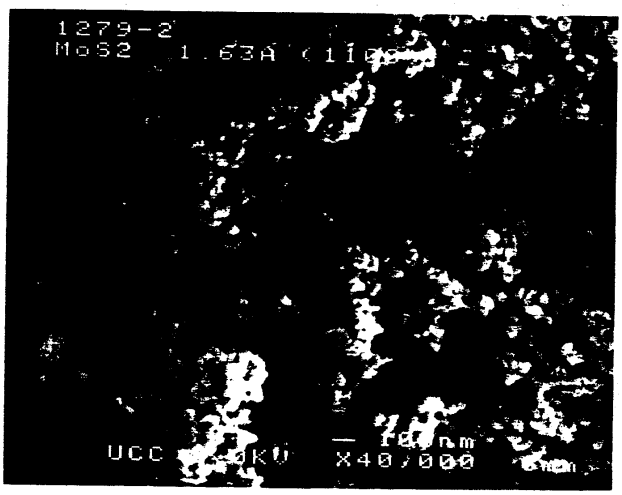

Figure 3. Scanning electron micrographs (40,000x) of the MoS_2 samples produced by the GPD reactions of $Mo(CO)_6$ and H_2S at (a) 500 C and (b) 1100 C using reactor configuration A.

MoS_2 particles in these samples are agglomerated and individually exhibit dimensions well-below 100 nm. Similar morphological features are evident in the corresponding SEMs of samples A2 and A3, which are not shown. As the reaction temperature increased, the products became more crystalline. The narrowing of the X-ray diffraction peaks (Figure 4) due to MoS_2 is consistent with a concomitant increase in crystallite grain size.

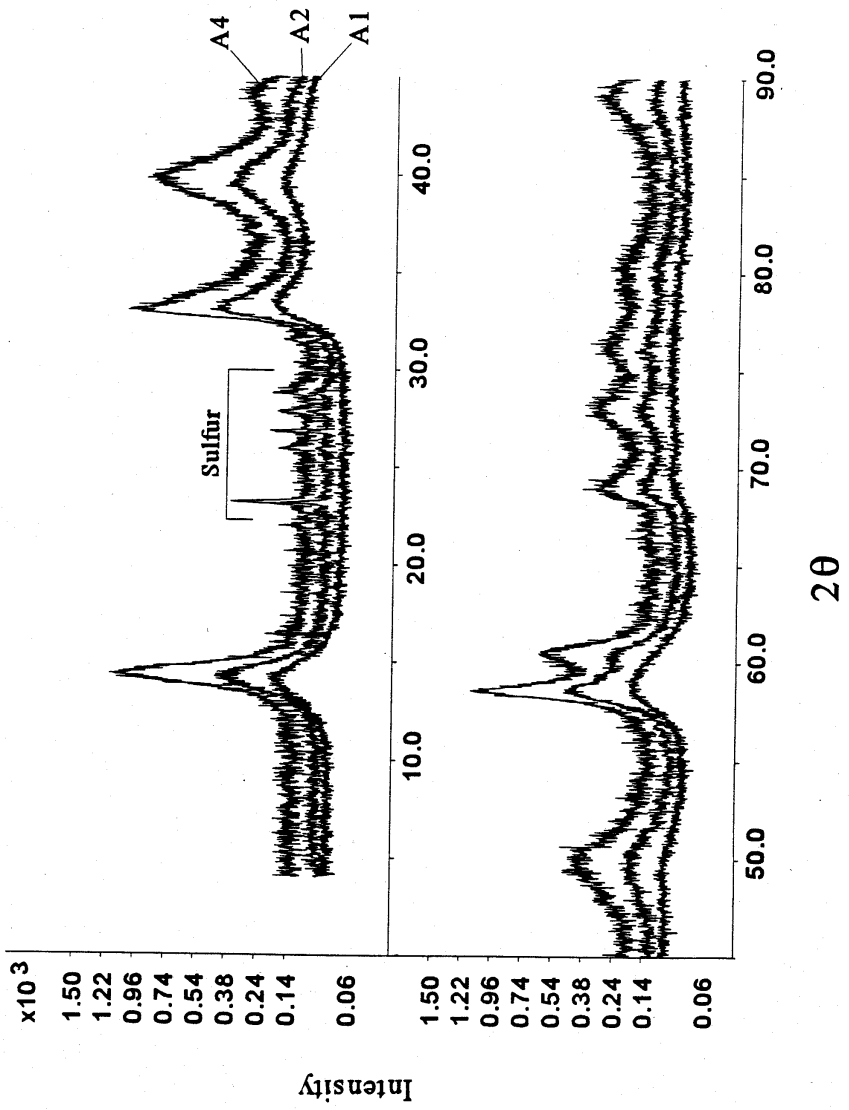

Figure 4. X-ray powder diffraction patterns for materials prepared by the thermal decomposition of $Mo(CO)_6$ and H_2S at 500 (A1), 800 (A2), and 1100 C (A4). A3 omitted for clarity.

The results of the XPS analyses performed on samples A1, A2, and A4 show that the S:Mo ratio near the surface is consistent with that found for MoS_2. Bulk sulfur analyses of these compounds, however, gave nominal molecular formulas of $MoS_{1.9}$, $MoS_{3.95}$, $MoS_{2.84}$, and $MoS_{2.92}$ for products A1 - A4, respectively. The excess sulfur in samples A2 - A4 corresponds to elemental sulfur, which was observed in the X-ray diffraction patterns and verified by the S 2p peaks corresponding to elemental sulfur in the respective XPS spectra. For sample A1 the only phase observed in the X-ray diffraction powder pattern was MoS_2, although a very small peak due to elemental sulfur was found in the S 2p XPS spectrum. The Mo and S binding energies for A1, A2, and

A4 matched those expected for MoS_2 (S 2p: 162.1 eV, 163.2 eV; Mo 3d: 229.2 eV, 232.4 eV).[17] The carbon composition for each of these compounds was less than 0.05 %, whereas surface oxygen was detected by XPS at levels ranging from 7-28%. Therefore, on the basis of the elemental analyses, the XRD powder diffraction patterns, and the XPS data, the only identifiable products were surface oxygen, elemental sulfur, and 2H-MoS_2.[18]

$Mo(CO)_6/H_2S$ Decompositions with Reactor Configuration B. This second series of GPD reactions focused on investigating the influence of specific reactor variables on the properties of the products. Specifically, variations in the furnace temperature, the $Mo(CO)_6$ partial pressure, or the inert gas flow rate produced significant changes (Table 3) in the surface

Table 3. Analytical Data for the MoS_2 Samples Prepared by the GPD of $Mo(CO)_6$ and H_2S with Reactor Configuration B.

Run	T_f[a]	Binding Energies (ev)				S/Mo (XPS)	Yield %	XRD[b] FWHH	Surface Area (m^2/g)	Sulfur % (Carbon %)
		Mo $3d_{3/2}$	Mo $3d_{5/2}$	S $2p_{1/2}$	S $2p_{3/2}$					
B1	300	231.5	228.5	162.8	161.9	0.88	26.7	5.4	21.4	22.6 (0.21)
B2	400	232.1	229.0, 228.2	162.9	162.0	0.86	45.2	5.6	47.3	22.4 (0.09)
B3	500	232.4	229.3	163.2	162.2	1.30	82.7	3.7	76.5	37.85 (0.04)
B4	600	232.5	229.3	163.3	162.2	1.59	88.6	2.6	75.4	42.61 (0.01)
B5	700	232.5	229.3	163.3	162.2		95.0	2.1	78.0	45.95 (<0.01)
B6	800	232.5	229.3	163.3	162.2		94.6	1.8	72.5	45.56 (0.06)
B7	900	232.5	229.3	163.3	162.2		98.2	1.5	66.2	46.03 (<0.01)

[a] T_f = furnace temperature.
[b] Full width at half height measurement in 2 for the Bragg powder diffraction peak for the(0 0 2) reflection.

area, chemical composition, and crystallite grain size of the product.

The influence of the reaction temperature on the product surface area was evaluated by decomposing $Mo(CO)_6/H_2S$ mixtures at temperatures ranging from 300-900 C (B1 - B7) and determining the surface areas of the isolated products with BET methods. The surface areas for these samples reached a maximum (75.4-78.0 m^2/g) within the temperature range of 500-700 C and then decreased at higher and lower temperatures. Molybdenum 3d and sulfur 2p binding energies for samples B1 - B4 were measured by X-ray photoelectron spectroscopy to monitor product composition. The sulfur 2p and the molybdenum 3d binding energies increased as the furnace temperature was elevated from 300 to 500 C and then remained unchanged for samples prepared at or above 600 C. The narrowing of the XRD peak widths observed in the XRD patterns (Figure 5) indicates that the reactor temperature also has a significant effect on the

crystallinity of the GPD product. As the reactor temperature increased from 300 to 900 C, the Bragg diffraction peaks due to MoS_2[17] emerged and continued to sharpen.

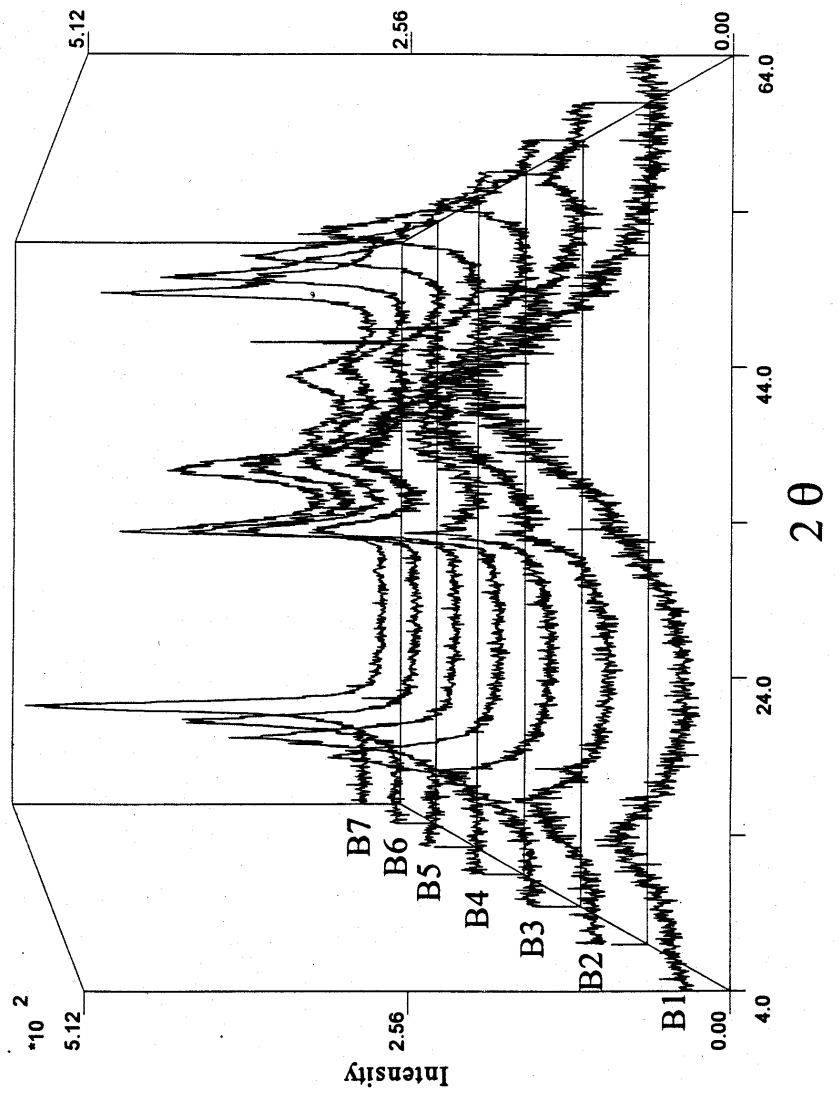

Figure 5. X-ray powder diffraction patterns of MoS_2 formed by the thermal decomposition of $Mo(CO)_6$ and H_2S at 300 (B1), 400 (B2), 500 (B3), 600 (B4), 700 (B5), 800 (B6), and 900 C (B7).

The influence of the $Mo(CO)_6$ partial pressure on the surface area, composition, and crystallinity of the molybdenum sulfide products was examined by varying the temperature used to heat the $Mo(CO)_6$ reservoir while keeping the reactor temperature constant at 500 C. Three compounds were prepared with the $Mo(CO)_6$ sample reservoir heated to 93 (B8), 98 (B3) and 104 C (B9). Sample B9 exhibited the lowest surface area (55.4 m^2/g), whereas sample B8 showed the highest surface area (95.1 m^2/g). The Mo 3d

and S 2p binding energies varied only slightly (0.1 to 0.3 eV). Although the product yields were essentially the same, the crystallinity of these three samples noticeably increased with an increase in the temperature used to sublime $Mo(CO)_6$.

The effect of varying the Ar flow rate through the inner tube of the water-cooled injector used for reactor configuration B was also examined. Three separate reactions were conducted. For reaction B10 the Ar flow rate was set at 0 with the H_2S flow rate at 15 mL/min. This reaction produced a molybdenum sulfide product with the highest surface area (120.5 m^2/g). Increasing the Ar flow rate from 0 mL/min to 220 mL/min (B3) led to a decrease in the surface area to 76.5 m^2/g and a significant increase in the product yield from <20 % to 82.7 %. For reaction B11 the small increase in the Ar flow rate resulted in decreases in the product surface area and product yield. The Mo 3d and S 2p binding energies were comparable for samples B10 and B11.

Mo_2S_3 Preparations. By lowering the H_2S flow rate (i.e., raising the Mo:S ratio) relative to those used to produce samples A1-B11, a lower valent molybdenum sulfide phase, Mo_2S_3, was produced. For reaction C1, the GPD of $Mo(CO)_6$ and H_2S (5 mL/min) at 1000 C afforded a material containing both MoS_2 and Mo_2S_3. These two phases were the only ones observed in the XRD patterns. For reaction C2, the lowering of the H_2S rate to 2.5 mL/min led to the observation of Mo_2S_3, MoS_2, and Mo. Not only was elemental molybdenum identified in the XRD, but the MoS_2:Mo_2S_3 ratio decreased, as indicated by the relative intensities of the Bragg diffraction peaks assignable to these two phases.

Discussion of Results

Influence of Furnace Temperature on Product Composition. The furnace temperature used to perform the GPD reactions $Mo(CO)_6$ and H_2S significantly influences the product composition, surface area, and crystallite size. Over the temperature range of 300-1100 C, the formation of MoS_2 is favored thermodynamically. In fact, due to the high thermodynamic stability of MoS_2, substitution of $Mo(CO)_6$ with a different molybdenum precursor, such as Mo_2C, MoC, MoO_2, Mo_2N, or MoN, still favors MoS_2 formation. The fact that MoS_2 is not produced at or below 400 C indicates that higher reaction temperatures are required to provide the activation energy needed to promote the production of MoS_2.

The two molybdenum sulfide materials, B1 and B2, prepared at 300 and 400 C, respectively, differ significantly in their chemical composition and molybdenum valency relative to sample B3 produced at 500 C. Whereas samples B1 and B2 exhibit an average bulk % sulfur of 22.5 %, corresponding to a S:Mo ratio near 1:1, sample B3 has a bulk % sulfur of 37.8 %, corresponding to a S:Mo ratio of 1.8. The Mo 3d binding energies measured for B1 ($3d_{5/2}$=228.5 eV; $3d_{3/2}$=231.5 eV) and B2 ($3d_{5/2}$=228.2 eV and 229.0 eV; $3d_{3/2}$=232.1 eV) are intermediate to those found for MoS_2 ($3d_{5/2}$=229.5 eV; $3d_{3/2}$=232.6 eV)[17] and Chevrel phase compounds, $M'Mo_6S_8$, where M'=Fe, Ni, Co, Pb, Sn and Ag (227.3 eV Mo $3d_{5/2}$ 228.2 eV).[19] In contrast, the Mo 3d binding energies measured for B3 ($3d_{5/2}$ = 229.3 eV; $3d_{3/2}$=232.4 eV) are in close agreement with the values reported for MoS_2. On the basis of these Mo 3d binding energies measured for B1 and B2, the corresponding formal Mo oxidation state in these samples lies between +2 (highly reduced Chevrel phase compounds) and +4 (MoS_2).

An initial concern was that the molybdenum sulfide compounds formed by $Mo(CO)_6$ decomposition might contain copious amounts of carbon and oxygen from inclusion of the carbonyl ligand. Based on the results of our compositional analyses, this did not occur. The highest carbon content found for these materials was 0.21% for sample B1.

In addition to the lower sulfur content and the lower formal Mo oxidation state associated with B1 and B2, the XRD data for these samples indicate the presence of limited atomic ordering. Estimates of the grain size in B1 (or B2) and B3 were obtained by application of the Scherrer equation for XRD peak broadening due to particle size effects. Using a Scherrer constant of unity, the sizes of the crystallite particles in B1 and B3 are estimated to be 1.6 and 3.2 nm, respectively. These dimensions are calculated with the assumption that the crystallite grain size is the primary factor contributing to the peak broadening. However, if appreciable lattice strain is present in these compounds, the grain size contribution to peak broadening is less.

The reaction temperature also has a strong influence on the surface areas of the GPD products, with the higher surface areas being obtained for the MoS_2 formed within the temperature range of 500 to 700 C. Although elemental sulfur was identified by XPS and XRD in bulk samples prepared at temperatures above 500 C, MoS_2 was the only molybdenum sulfide compound present. The Mo 3d and S 2p binding energies of the materials prepared at or above 500 C are consistent with the Mo and S binding energies found for MoS_2. Although the relative peak intensities do not match those found in the JCPDS file for 2H-MoS_2,[17] the XRD peak positions match exactly those for this hexagonal phase of MoS_2. The intensity differences are primarily observed for the (0 0) planes, suggesting the apparent discrepancy may be a consequence of preferred orientation effects. In view of the observed broadening of the XRD peaks, the co-existence of the 3R-MoS_2[18] phase, however, cannot be ruled out.

As the decomposition temperature is raised from 500 to 1100 C, the surface area of the resultant product generally decreases with a concomitant increase in the crystallinity. Although similar property trends are observed for MoS_2 produced with reactor configurations A and B, the difference in the magnitude of the surface area variation with reaction temperature for these two configurations is worth noting. For reactor configuration A, the surface area decreases from 82.0 (A1, 500 C) to 16.7 m^2/g (A4, 1100 C), respectively. This inverse correlation between the MoS_2 surface area and the furnace temperature is complicated by the additional sulfur present in samples A2, A3, and A4 as rhombohedral S_8. However, the XRD pattern measured for these samples indicates that S_8 in these samples is highly crystalline, thereby suggesting that the sulfur contribution to the surface area measurements is minimal (i.e., less than 1 m^2/g). Thus, the observed reduction in the measured surface area is probably not due to the excess sulfur present, but actually reflects the lower surface areas of the MoS_2 present in these four samples.

Whereas a significant decrease in the surface area was observed with increasing reactor temperature for the samples prepared using reactor configuration A, the surface areas of the corresponding MoS_2 materials generated using reactor configuration B remained fairly constant, ranging from 78.0 m^2/g at 500 C to 66.2 m^2/g at 900 C. This modest surface area variation is attributed almost entirely to the changes in the MoS_2 surface area and not to the presence of excess elemental sulfur. The residual sulfur

present in samples B6-B9 ranges from three to nine weight percent, therefore suggesting that the actual surface areas of the MoS_2 in these samples may be somewhat higher than the experimental values reported in Table 3.

In these GPD reactions there are at least three fundamental process variables that directly influence the product surface area. These factors include the relative rate of the GPD reaction, the degree of annealing of the solid particles formed, and the initial composition of the $Mo(CO)_6/H_2S$ mixture in the gas phase. The furnace temperature obviously affects the first two process variables, whereas the third can be altered by changing the $Mo(CO)_6$ reservoir temperature, the H_2S flow rate, and the inert gas flow rates over the $Mo(CO)_6$. One might expect that increasing the reactor temperature will increase both the rate of the GPD reaction and the degree of annealing of the MoS_2 particles. The higher rate of decomposition associated with a higher furnace temperatures should afford more finely divided material, analogous to liquid precipitation reactions where the particle size is controlled by the kinetics of the decomposition.[20] On the other hand, because these products are comprised of agglomerated particles (Figure 3), an increase in the reactor temperature would also be expected to increase the solid state diffusion rates, thus producing larger particles with lower surface areas. Consequently, these two opposing effects directly influence the bulk surface area as the reactor temperature is increased.

Reactor configurations A and B further differ in the way the gaseous reactants are introduced into the hot zone and the distance through which the solid particulate is heated. With reactor configuration A, the gaseous reactants after they exit the injector inlet are exposed to a significant temperature gradient within the tube furnace prior to reaching the reactor's process temperature. In contrast, reactor configuration B facilitates the introduction of reactant vapors into the central section of the furnace hot zone where the temperature gradient over a six inch length is 5 C. This alternative configuration provides better control over the temperature of the decomposition event and the heating length. By taking into consideration the differences in the gas flow rates and the heating distances used for these two reactor configurations, the annealing time for configuration A is estimated to be approximately three times longer than that for configuration B. This reduction in heating/annealing time may be the primary reason why the surface areas of the MoS_2 samples prepared with reactor configuration B do not vary significantly with reaction temperature.

A significant reduction in the heating/annealing time during a gas phase decomposition reaction has been realized when laser excitation is used to initiate the reaction.[21] Because the effective reaction volume is limited by the dimensions of the laser beam, products pass quickly out of the reactor, thereby minimizing annealing effects on the particle size. Although resistive heating methods cannot easily duplicate the decomposition event produced by lasers, the results of this study show that simple modifications of the reactor configuration can reduce significantly post-decomposition heating effects and increase the reaction yields to those approaching the theoretical limit.

Influence of $Mo(CO)_6$ Reservoir Temperature and Carrier Gas Flow Rates on Product Composition. The $Mo(CO)_6$ reservoir temperature and the carrier gas flow rate over the $Mo(CO)_6$ can be used to modify the product composition and bulk properties. An increase in either the temperature used to heat the $Mo(CO)_6$ reservoir or the rate of Ar flow through the reactor resulted in lowering the surface area and

crystallinity of the molybdenum sulfide product(s) at a given reactor temperature. Although the limits of these process variables remain to be investigated, the analytical data summarized in Tables 4 and 5 demonstrate that the surface area of the MoS_2 can be doubled by making relatively small changes in the $Mo(CO)_6$ temperature and the Ar flow rate.

Table 4. Analytical Results for the MoS_2 Samples Prepared by Varying the $Mo(CO)_6$ Reservoir Temperature.

Run	T_{Mo}[a]	Binding Energies (ev)				S/Mo Ratio (XPS)	Yield %	XRD[b] FWHH	Surface Area	Sulfur % (Carbon %)
		Mo $3d_{3/2}$	Mo $3d_{5/2}$	S $2p_{1/2}$	S $2p_{3/2}$					
B8	93	232.6	229.4	163.2	162.3	1.68	82.8	3.2	95.1	41.32 (<0.01)
B3	98	232.4	229.3	163.2	162.2	1.30	82.7	3.7	76.5	37.85 (0.04)
B9	104	232.3	229.2	163.1	162.1	1.04	82.8	5.7	55.4	32.70 (0.04)

[a] Temperature of the $Mo(CO)_6$ reservoir.
[b] Full width at half height measurement in 2 of the Bragg diffraction peak for the (0 0 2) reflection.

Table 5. Analytical Results for the MoS_2 Samples Prepared by Varying Argon Gas Flow Rate.

Run	Ar_i[a] Rate	H_2S Rate	Binding Energies (ev)				S/Mo Ratio (XPS)	Yield %	XRD[b] FWHH	Surface Area	Sulfur % (Carbon %)
			Mo $3d_{3/2}$	Mo $3d_{5/2}$	S $2p_{1/2}$	S $2p_{3/2}$					
B10	0	15						<20		120.5	N/A
B3	220	11	232.4	229.3	163.2	162.2	1.30	82.7	3.7	76.5	37.85 (0.04)
B11	250	11	232.3	229.2	163.1	162.2	1.01	75.5	5.3	64.0	34.09 (<0.01)

[a] Argon flow rate through the inner tube of reactor configuration B.
[b] Full width at half height measurement in 2 for the Bragg powder diffraction peak of the (0 0 2) reflection.

Mo_2S_3 Preparations. We have shown by the use of a low H_2S flow rate (i.e., at or below 5 mL/min) that it is possible to produce the reduced phase, Mo_2S_3, at 1000 C by a GPD reaction. Alternatively, when the H_2S flow rate equals or exceeds the stoichiometric amount needed to produce MoS_2, the only molybdenum containing phase observed in the XRD is 1H-MoS_2.[18] However, it should be pointed out that due to the nature of the reactor geometry the amount of $Mo(CO)_6$ in the reactive gas stream decreases as the $Mo(CO)_6$ in the reservoir is consumed during the course of the reaction. Consequently, at fixed H_2S flow rates at or below 5.0 mL/min, Mo_2S_3 (C1) or Mo_2S_3 and Mo metal (C2) are formed primarily at the beginning of the reaction when the $Mo(CO)_6$ concentration is high. However, as this concentration decreases, more MoS_2 is generated during the latter stages of these reactions.

The results for reactions C1 and C2 further suggest that it may be possible to obtain pure phase Mo_2S_3 by modifying the $Mo(CO)_6$ section of the reactor to facilitate a constant introduction of $Mo(CO)_6$ vapor. Further, the controlled introduction of another volatile metal carbonyl, such as $Fe(CO)_5$, into the reactive gas stream containing $Mo(CO)_6$ and H_2S, may provide the opportunity to produce other molybdenum sulfide phases, such as Chevrel phase compounds, M'Mo_6S_8 (M'=Fe, Ni, Co, etc.), some of which are also known to catalyze hydrodesulfurization reactions.[18] However, due to the conventional solid state methods employed to produce these compounds, their surface areas are typically close to 1 m^2/g. Chevrel and his co-workers have speculated about the viability of preparing supported Chevrel phase compounds from soluble precursors.[22] However, lower reaction temperatures will be necessary to avoid subsequent reduction in the surface area of the support by sintering processes. Therefore, the major hurdles that must be overcome in order to prepare high surface area Chevrel phase compounds via a GPD reaction are the precise control of the composition of the reactive gas stream and the minimization of annealing effects induced by heating at high temperatures.

The feasibility of using our continuous flow gas phase reactor to prepare bimetallic ternary materials, however, has been demonstrated recently in our laboratories. Preliminary studies have demonstrated that the thermal decomposition of gaseous mixtures of $Fe(CO)_5$, $Mo(CO)_6$, and ammonia lead to the production of solid solutions in

which the Fe in -Fe_3N is partially substituted by molybdenum, as verified by EDS measurements and the expanded dimensions of its hexagonal lattice.[23]

Concluding Remarks

A continuous flow reactor has been developed for the production of molybdenum sulfide compounds by the gas phase decomposition of $Mo(CO)_6$ and H_2S. Nanoscale MoS_2 solids with surface areas ranging from 16 to 120 m^2/g were generated over the temperature range, 500-900 C, while lower valent molybdenum sulfides were obtained at 300 and 400 C. Three critical catalyst properties - the surface area, the chemical composition, and the crystallographic phase - were controlled by varying the furnace temperature, the carrier gas flow rate, and the partial pressure of the $Mo(CO)_6$ used in these GPD reactions. By modifying the original reactor with a water-cooled injector to induce laminar gas flow around the reactive gases, product yields were increased from 40-64 % to 75-98%. In addition to MoS_2, microcrystalline Mo_2S_3 was produced by lowering the H_2S flow rate. These high surface area MoS_2 materials, when promoted with alkali, have been subsequently shown[24] to exhibit high catalytic activity for the selective production of linear alcohols from synthesis gas. Although this study focuses on the preparation of molybdenum sulfides, molybdenum nitrides and mixed metal nitrides have been prepared in this continuous flow reactor by the decomposition of $Mo(CO)_6/NH_3$ vapors and by the introduction of $Fe(CO)_5$ into this reactive gas stream, respectively.[23]

Acknowledgment. Special appreciation to undergraduate students Michael Delancey and Damian Huff for the preparation and X-ray analyses. We also thank Professor John Renton for assistance with X-ray powder studies and Ghaleb Salaita at Union Carbide Corporation for the XPS analyses.

References

(1) Hitchman, M. L.; Jensen, K. F. *Chemical Vapor Deposition: Principles and Applications*; Academic Press: London, 1993.

(2) (a) Rao, C. N. R.; Gopalakrishnan, J. *Acc. Chem. Res*. **1987**, 20, 228. (b) Livage, J. *J. Solid State Chem*. **1986**, 64, 322. (c) Shibata, S.; Kitagawa, T.; Okazaki, H.; Kimuait, T.; Murakami, T. *Jap. J. Appl. Phys*. **1988**, 27, L53. (d) Livage, J.; Lemerle, J. *Ann. Rev. Mater. Sci*. **1982**, 12, 103. (e) Hench, L. L.; West, J. K. *Chem. Rev*. **1990**, 90, 33 and references cited therein.

(3) (a) McHale, R. W.; Schaeffer, R. W.; Kebede, A.; Macho, J.; Salomon, R. E. *J. Supercond*. **1992,** 5, 511. (b) Arya, S. P. S.; Hintermann, H. E. *Thin Solid Films* **1990**, 193, 841. (c) Cooper, E. I.; Giess, E. A.; Gupta, A. *Mater. Lett*. **1988**, 7, 5. (d) Gupta, A.; Koren, G.; Giess, E. A.; Moore, N. R.; O'Sullivan, E. J. M.; Cooper, E. I. *Appl. Phys. Lett*. **1988**, 52, 163.

(4) (a) Kumar, P.; Pillai, V.; Shah, D. O. *Appl. Phys. Lett.* **1993**, 62, 765. (b) Zhang, Y.; Muhammed, M.; Wang, L.; Nogues, J.; Rao, K. V. *Mater. Chem. Phys*. **1992**, 32, 213. (c) Spencer, N. D. *Chem. Mater*. **1990**, 2, 708.

(5) Kasztelan, S.; Wambeke, A.; Jalowiechi, L.; Grimblot, J.; Bonnelle, J. P. *J. Catal*. **1990**, 124, 12.

(6) (a) Pecararo, T. A.; Chianelli, R. R. *J. Catal*. **1981**, 67, 430. (b) Chianelli, R. R.; Pecoraro, T. A.; Halbert, T. R.; Pan, W.-H.; Stiefel, E. I. *J. Catal*. **1984**, 86, 226. (c) Gobolos, S.; Wu, Q.; Delannay, F.; Grange, P.; Delmon, B.; LaDriere, J. *Polyhedron* **1986**, 5, 219. (d) Lindner, J.; Sachdev, A.; Villa Garcia, M. A.; Schwank, J. *J. Catal*. **1989**, 120, 487.

(7) (a) Gavin, D. G.; Richards, D. G. GB 2-185-907-A, filed 2/4/86 (published 8/5/87), assigned to Coal Industry Limited. (b) Quarderer, G. J.; Cochran, G. A. US 4,749,724, filed 11/20/86 (published 6/7/88), assigned to The Dow Chemical Company. (c) Stevens, R. R.; Conway, M. M. US 4,831,060, filed 6/6/88 (published 5/16/89), assigned to The Dow Chemical Company. (d) Kinkade, N. E. US 4,590,314, filed 11/19/84 (published 5/20/86), assigned to Union Carbide Corporation. (e) Kinkade, N. E. US 4,994,498, filed 3/2/90 (published 2/19/91), assigned to Union Carbide Corporation. (f) Klier, K.; Herman, R. G.; Simmons, G. W.; Lyman, C. E.; Santiesteban, J. G.; Najbar, M.; Bastian, R. Report, 1990, DOE/PC/13580-1; Order no. DE89009888.

(8) Eggersen, F. T.; Roberts, R. M. *J. Phys. Chem*. **1959**, 63, 1981.

(9) Wildervanck, J. C.; Jellinck, F. *Z. Anorg. Allg. Chem*. **1964**, 328, 309.

(10) (a) Bonneau, P. R.; Jarvis, R. F., Jr.; Kaner, R. B. *Nature* **1991**, 349, 510.
(b) Bonneau, P. R.; Wiley, J. B.; Kaner, R. B. *Inorg. Synth.* **1995**, 30, 33.

(11) (a) Oyama, T.; Ishii, T.; Takeuchi, K. *Kazuo Reza Kenkyu* **1994**, 22, 2. (b) Oyama, T.; Takehisa, K.; Ishii, T.; Takeuchi, K. *Reza Kagaku Kenkyu* **1989**, 11, 90. (c) Ochoa, R.; Hager, G. T.; Lee, W. T.; Bandow, S.; Givens, E.; Eklund, P. C. *Mater. Res. Soc. Proc*. **1995**, 368, 27.

(12) (a) Rice, D. A.; Hibble, S. J.; Almond, M. J.; Mohammad, K. A. H.; Pearse, S. P. *J. Mater. Chem.* **1992**, 2, 895. (b) Chatzitheodorou, G.; Fiechter, S.; Kunst, M.; Luck, J.; Tributsch, H. *Mater. Res. Bull*. **1988**, 23, 1261.

(13) (a) Suhr, H.; Schmid, R.; Stuermer, W. *Plasma Chem. Plasma Process*. **1992**, 12, 147. (b) Suhr, H.; Schmid, R.; Traus, I. DE 3834356 A1, filed Oct. 6, 1988 (published April 12, 1990), assigned to Schering A.-G.

(14) Feldman, Y.; Wasserman, E.; Srolovitz, D. J.; Tenne, R. *Science* **1995**, *267*, 222.

(15) Kugler, E. L.; Zubovic, E., personal communication.

(16) Zero background single crystal quartz disks obtained from: Gem Dugout, 1652 Princeton Dr., State College, PA, 16803.

(17) Stevens, G. C.; Edmonds, T. *J. Catal*. **1975**, 37, 544.

(18) These phase designations are used in the JCPDS (Joint Committee for Powder Diffraction Studies, International Center for Diffraction Data, Swarthmore, PA) database. X-ray powder diffraction data for 2H-MoS_2 and for 3R-MoS_2 are found in JCPDS Card # 6-97, and JCPDS Card # 17-744, respectively.

(19) (a) McCarty, K. F.; Anderegg, J. W.; Schrader, G. L. *J. Catal*. **1985**, 93, 375. (b) Ekman, M. E.; Anderegg, J. W.; Schrader, G. L. *J. Catal*. **1989**, 117, 246.

(20) (a) Henglein, A. *Chem. Rev.* **1989**, 89, 1861. (b) Rossetti, R.; Hull, R.; Gibson, J. M.; Brus, L. E. *J. Chem. Phys.* **1984**, 82, 552.

(21) (a) Haggerty, J. S. *Sinterable Powders from Laser-Driven Reactions* in *Laser-induced Chemical Processes*, ed., Steingeld, J. I., Plenum Press: New York, 1981.
(b) Rice, G. W. *Laser Driven Synthesis if Transition-Metal Carbides, Sulfides, and Oxynitrides* in *Laser Chemistry of Organometallics*, 1993.

(22) (a) Rabiller-Baudry, M.; Sergent, M.; Chevrel, R. *Mater. Res. Bull*. **1991**, 26, 519.
(b) Rabiller-Baudry, M.; Chevrel R.; Sergent, M. *J. Alloys Comp*. **1992**, 178, 441.

(23) Close, M. R.; Petersen, J. L. *Mater. Res. Soc. Proc*. **1995**, 368, 33

(24) Liu, Z.; Li, X.; Close, M. R.; Kugler, E. L.; Petersen, J. L.; Dadyburjor, D. B. *Ind. Eng. Chem. Res.* **1997**, 36, 3085.